ELSEVIER

CrossMark

Hydrogen generation from hydrous hydrazine over Ni/CeO$_2$ catalysts prepared by solution combustion synthesis

Wooram Kang, Arvind Varma*

Davidson School of Chemical Engineering, Purdue University, 480 Stadium Mall Drive, West Lafayette, IN 47907, USA

ARTICLE INFO

ABSTRACT

Hydrous hydrazine is a promising hydrogen carrier for fuel cell vehicles owing to its high hydrogen content (8.0 wt% for N$_2$H$_4$·H$_2$O), low cost and stable liquid state at ambient temperature. The development of cost effective catalysts with high activity and 100% selectivity for hydrogen generation under mild conditions, however, is a significant challenge for its practical use. In this work, a series of Ni/CeO$_2$ catalysts were prepared by solution combustion synthesis (SCS), varying the SCS parameters in terms of ratio of precursor oxidizers (nickel nitrate and ammonium cerium nitrate), fuel-to-oxidizer ratio (0.5–3) and fuel type (hydrous hydrazine and glycine). These parameters influence the combustion behavior and, in turn, the physicochemical properties of catalysts such as crystallinity, Ni particle size, surface area and pore size as well as formation of Ni−O−Ce solid solution. The reaction mechanism for the SCS process is discussed. The tailored 6 wt% Ni/CeO$_2$ catalyst synthesized with fuel-to-oxidizer ratio 2 and hydrous hydrazine fuel, exhibited 100% selectivity for hydrogen generation and good activity with a TOF value 34.0 h^{-1} at 50 °C, which is the highest catalytic performance among all prior reported catalysts containing Ni alone.

1. Introduction

Hydrogen is a promising energy carrier since its gravimetric energy density (120 MJ/kg) is higher than conventional hydrocarbon fuels such as gasoline and diesel, with the added benefit that its combustion product, water, is environmentally benign. Hydrogen, however, is the lightest gas, hence it has poor volumetric energy density (0.01 MJ/L at STP), which presents significant difficulty in storing large quantity of hydrogen for vehicle and portable applications. Accordingly, finding an efficient hydrogen storage material is among the main challenges for the development of on-board hydrogen storage applications. Over the past decades, various hydrogen storage materials (sorbents, metal hydrides, chemical hydrides) have been investigated extensively [1]. None of these materials, however, have been demonstrated to meet practical requirements such as volumetric and gravimetric hydrogen capacities, handling pressure and temperature, regeneration of spent product and cost [1,2].

Hydrous hydrazine such as hydrazine monohydrate (N$_2$H$_4$·H$_2$O) is a promising but not well explored hydrogen carrier for storage and transportation applications owing to its high hydrogen content (8.0 wt %), low material cost and capability of generating hydrogen at room temperature [3,4]. In particular, its stable liquid state over a wide range of temperature (221–393 K) presents advantages for easy recharging

and potential availability of current infrastructure for liquid fuels. In addition, generation of only nitrogen as byproduct obviates the need for on-board collection for spent fuel regeneration.

Basically, hydrogen can be generated from hydrazine decomposition which proceeds by two different reaction pathways: the complete decomposition [N$_2$H$_4$ (l) → N$_2$ (g) + 2H$_2$ (g)] and the incomplete decomposition [3N$_2$H$_4$ (l) → 4NH$_3$ (g) + N$_2$ (g)]. Notably, since only the complete decomposition leads to hydrogen generation and even small amount of ammonia as byproduct is poison for hydrogen fuel cells [5,6], the development of efficient and selective catalysts, which enhance the complete decomposition and simultaneously suppress the incomplete decomposition, is important. Towards this aim, many catalysts containing noble (Ir, Rh, Pd and Pt) and transition metals (Ni, Fe, Co and Cu) have been investigated for efficient catalytic decomposition of hydrous hydrazine [7–14]. Among these, Ni-based catalysts exhibit superior catalytic activity and selectivity for hydrogen generation. Recent studies also show that the use of metal oxides (Al$_2$O$_3$, CeO$_2$, La$_2$O$_3$ and MnO$_2$) as supports significantly enhances catalyst performance by providing high metal surface area and strong metal-support interaction [15–22].

This study is focused for the first time on a non-conventional one-step method, namely solution combustion synthesis (SCS), as the preparation method of cost effective metal catalysts supported on metal

---

oxide for decomposition of hydrous hydrazine. SCS is a self-sustained process where the main source of energy is the combustion reaction between a metal oxidizer and a fuel. In general, since the combustion reaction is completed within a short time, various products (e.g., metals, metal oxides, alloys and sulfides) can be obtained simply and rapidly [23]. Also, the mixing of precursors in aqueous solution at the molecular level and the generation of gaseous byproducts during combustion allow the formation of nanoscale powders with uniform composition and high metal dispersion. It has been noted that physical properties of the resulting products depend strongly on combustion characteristics which are mainly determined by the synthesis parameters such as the nature of fuel, metal oxidizer, and fuel-to-oxidizer ratio [24–31]. Although many prior studies used SCS to prepare metal or metal oxides for various applications, there are relatively few reports describing the quantitative effects of synthesis parameters on the physical and catalytic properties of catalysts.

In this work, Ni/CeO_2 catalysts, as a representative of metal catalysts supported on metal oxide, are prepared by SCS in a one-step process by varying the synthesis parameters to develop efficient catalysts for decomposition of hydrous hydrazine. The characterization and testing of the Ni/CeO_2 catalysts were conducted to understand the effects of the synthesis parameters on the SCS process and its correlation with the physical and catalytic properties. Finally, the catalytic performance of the Ni/CeO_2 prepared by SCS was compared with that of catalysts prepared by different prior methods.

2. Experimental

2.1. Catalyst preparation

The SCS was used for preparation of all the studied catalysts in this work. In a typical experiment, stoichiometric amount of nickel nitrate hexahydrate [$Ni(NO_3)_2 \cdot 6H_2O$, Alfa Aesar, 98%] and cerium ammonium nitrate [$(NH_4)_2Ce(NO_3)_6$, Alfa Aesar, 98+%] as metal oxidizers were dissolved in a minimum amount of distilled water and then added to hydrous hydrazine ($N_2H_4 \cdot H_2O$, Alfa Aesar, 99+%) or glycine (NH_2CH_2COOH, Alfa Aesar, 99.5%) as fuel. The amounts of metal oxidizers were determined to prepare catalysts with different nickel loading (3–68 wt%). The Ni contents of the catalysts were determined by atomic absorption spectroscopy (Table S1). The amount of fuel was adjusted by the fuel-to-oxidizer ratio, ϕ and four values (0.5–3) were selected to investigate the effect of ϕ on the SCS behavior and properties of the resulting products. After thorough mixing of the obtained solution, the mixture was heated over a hot plate to induce the self-sustained combustion. Typically, after dehydration of the aqueous precursor solution, ignition occurred, leading to combustion along with large gas evolution. During combustion, the temperature abruptly increased to a maximum value, followed by rapid cooling due to gas evolution and heat loss to the surroundings (Fig. 1). The temperature change during combustion was monitored using an R-type thermocouple (tip diameter 0.125 mm) and the combustion behavior was also monitored by video recording. After cooling to room temperature, the resulting powders were calcined in air at 400 °C for 4 h and then treated at 400 °C for 1 h in a flow of 10 vol% hydrogen, balance argon, to reduce NiO to Ni. All the prepared catalysts are designated as x wt% Ni/CeO_2-y-z, where 'x' is the wt% of Ni present in the catalyst, 'y' is the type of fuel and 'z' is the ϕ value. For example, 6 wt% Ni/CeO_2-HH-2 denotes a Ni/CeO_2 catalyst with 5.8 wt% Ni loading, prepared with hydrous hydrazine as fuel and $\phi = 2$.

To calculate the adiabatic temperature for a given SCS condition and compare to the experimentally measured maximum temperature, thermodynamic calculations were conducted using the "Thermo" software package, which is based on the minimization of thermodynamic potential and includes properties of more than 2500 compounds [32]. The combustion reactions between metal oxidizers and fuel [Eq. (1) for hydrous hydrazine and Eq. (2) for glycine] considered for the
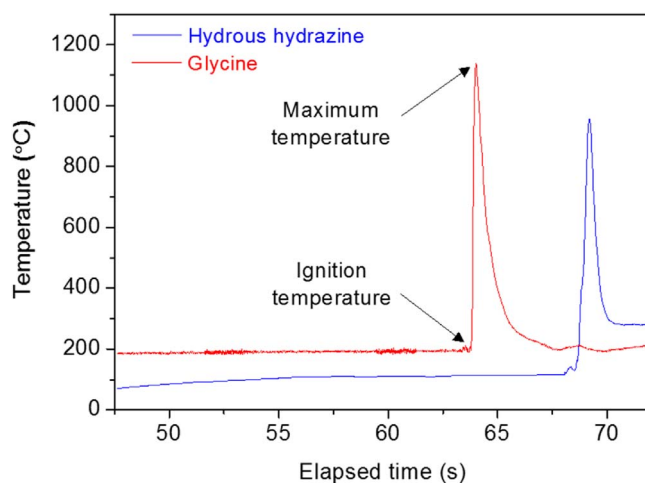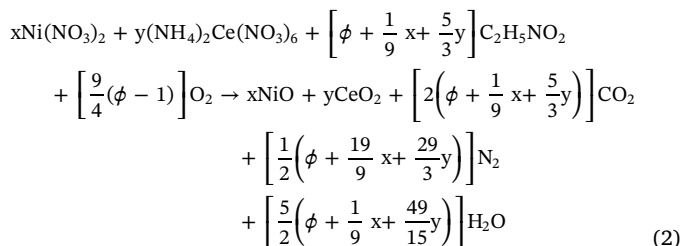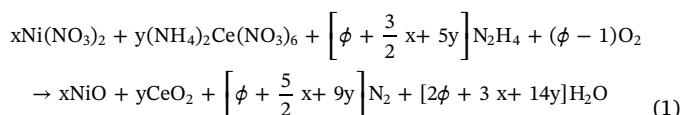

Fig. 1. Temperature-time profiles for SCS in hydrous hydrazine and glycine fuel systems.

thermodynamic calculations are shown below:

$$xNi(NO_3)_2 + y(NH_4)_2Ce(NO_3)_6 + \left[\phi + \frac{3}{2}x + 5y\right]N_2H_4 + (\phi - 1)O_2$$

$$\rightarrow xNiO + yCeO_2 + \left[\phi + \frac{5}{2}x + 9y\right]N_2 + [2\phi + 3x + 14y]H_2O \quad (1)$$

$$xNi(NO_3)_2 + y(NH_4)_2Ce(NO_3)_6 + \left[\phi + \frac{1}{9}x + \frac{5}{3}y\right]C_2H_5NO_2$$

$$+ \left[\frac{9}{4}(\phi - 1)\right]O_2 \rightarrow xNiO + yCeO_2 + \left[2\left(\phi + \frac{1}{9}x + \frac{5}{3}y\right)\right]CO_2$$

$$+ \left[\frac{1}{2}\left(\phi + \frac{19}{9}x + \frac{29}{3}y\right)\right]N_2$$

$$+ \left[\frac{5}{2}\left(\phi + \frac{1}{9}x + \frac{49}{15}y\right)\right]H_2O \quad (2)$$

where x and y are the number of moles of Ni and Ce, respectively. The number of moles of evolved gases per mole of product was calculated based on Eqs. (1) and (2).
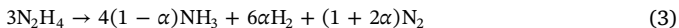
2.2. Catalyst characterization

X-ray diffraction (XRD) patterns were obtained using Rigaku SmartLab X-Ray Diffractometer with CuKα radiation (λ = 0.1541 nm) and a power 40 kV × 40 mA. The intensity data were collected by step-scanning over the range 20°–80° with a step of 0.02°. The specific surface area, total pore volume and average pore size of the catalysts were measured in a Quantachrome Autosorb by N_2 adsorption-desorption analysis using the multi-point BET method and BJH model. Prior to each measurement, the sample was degassed at 250 °C for overnight. The microstructure of samples was determined using a transmission electron microscope (TEM, FEI Tecnai G2 20). To prepare the TEM samples, the powder catalyst was first dispersed in water by ultrasound and then deposited on a copper grid coated with a holey carbon film. The mean particle size of Ni in catalysts was determined from the XRD patterns by the Scherrer equation and confirmed with TEM pictures. The Ni loading in the catalysts was measured using atomic absorption spectroscopy (AAS) on a PerkinElmer AAnalyst 300. The H_2 temperature programmed reduction (H_2-TPR) experiments were carried out with 200 mg NiO/CeO_2 sample packed in a stainless-steel column, using a Gow-Mac Model 20 thermal conductivity detector. Prior to TPR studies, N_2 gas was passed at 200 °C for 1 h to pretreat the sample and then cooled to room temperature. A 10 vol% H_2/N_2 mixture as reducing gas was flowed until the baseline of TCD signal became stable and then the sample temperature was increased at a constant 10 °C/min rate from room temperature to 700 °C. The amount of H_2 consumption as a

function of temperature was determined from the TCD signal.

2.3. Catalytic decomposition of hydrous hydrazine

The catalytic reactions were conducted in a stainless-steel reactor (Parr Instrument Company, Model 4592) with external heating, shown in Fig. S1. The reactor volume, including added fittings and tubing, was determined to be 63 ml. The catalyst was placed in a small glass vial (4 ml) inside the reactor, under argon (99.999%) atmosphere and then the reactor was preheated and held at the desired temperature (30–90 °C). Under magnetic stirring of 1100 rpm, the reaction was initiated by injecting 2 ml diluted hydrous hydrazine solution (0.4 M) with NaOH (0.5 M) into the vial containing the catalyst. In all cases, the molar ratio of Ni in the catalyst to hydrous hydrazine was kept fixed at 1:10. The agitation speed where the reaction rate was not controlled by external mass transfer was determined by preliminary experiments to be above 900 rpm, where the highest reaction temperature (90 °C) was tested because the mass transfer limitation would be the most severe (Fig. S2). The concentration of NaOH (Sigma-Aldrich, 50% in H_2O), which plays an important role in promoting the H_2 selectivity and kinetics of hydrous hydrazine decomposition [33–36], was optimized and the highest catalytic activity and H_2 selectivity were obtained in 0.5 M NaOH solution (Fig. S3). The reaction progress was monitored by measuring reactor pressure using a transducer (Omega Engineering PX35D1). After reaction completion, the product gas composition was analyzed by mass spectrometer (Hiden Analytical HPR-20) or micro gas chromatography (Agilent Micro GC 3000A), to obtain the molar ratio of N_2 to H_2 and to assess the presence of NH_3. The peak areas of H_2 and N_2 were calibrated using standard gas mixtures with different H_2/N_2 molar ratios.

The selectivity for hydrogen generation (α) was calculated based on the overall decomposition reaction (Eq. 3), leading to Eq. (4).

$$3N_2H_4 \rightarrow 4(1 - \alpha)NH_3 + 6\alpha H_2 + (1 + 2\alpha)N_2 \qquad (3)$$

$$\alpha = \frac{1}{6(n(N_2)/n(H_2)) - 2}, \quad (0 \leq \alpha \leq 1) \qquad (4)$$

The turnover frequency (TOF) values for the catalysts were calculated based on all the Ni atoms present, as follows:

$$TOF(h^{-1}) = \frac{n(H_2)}{n(Ni) \times t} \qquad (5)$$

where $n(H_2)$ is the moles of produced H_2, $n(Ni)$ is the moles of Ni in catalyst, and t is the reaction time for 50% conversion of hydrous hydrazine. The reported TOF values are averages from 2 to 5 experiments. To test recyclability of the catalyst, the reaction was repeated for three runs under the same conditions as the first cycle. After the hydrogen generation was completed, the catalyst was separated from the reaction solution by centrifugation, washed with water and tested under the same conditions.

3. Results and discussion

3.1. Combustion characteristics

The combustion characteristics including the measured maximum temperature, the calculated adiabatic temperature, and the amount of evolved gas during combustion for all catalysts studied are summarized in Table 1. The maximum temperature is an important system characteristic and relates to formation of products with desired crystallinity, although too high temperature may cause agglomeration and sintering of metal particles. The gas evolution during combustion dissipates the heat, inhibits agglomeration and promotes the porosity of products. As expected, the calculated adiabatic temperatures are always higher than the measured maximum temperatures. The discrepancy is due to non-adiabatic experimental conditions and possible delay of the

thermocouple signal. Nevertheless, the trends of the adiabatic temperature agree well with the measured maximum temperature.

The effect of different fuels on the combustion characteristics is shown in Fig. 2 and Table 1. Visually, combustion with glycine fuel (6 wt% Ni/CeO_2-GL-2) took place vigorously within the entire volume of the precursor mixture with high maximum temperature ($\sim$1150 °C) for a short duration ($\sim$2 s). On the other hand, combustion with hydrous hydrazine fuel (6 wt% Ni/CeO_2-HH-2) occurred with ignition locally followed by steady wave propagation along the mixture with moderate maximum temperature ($\sim$940 °C), lasting about 50 s until combustion was complete. The features of combustion with glycine and hydrous hydrazine fuels correspond to the volume combustion synthesis and the self-propagating high-temperature synthesis modes, respectively [23].

The lower measured maximum temperature for the hydrous hydrazine fuel, as compared to glycine, corresponds to the predictions for the adiabatic case (Table 1). The different ignition temperatures for the two fuels can be related to their distinct combustion mechanisms. As shown in Fig. 1, the glycine system ignited at $\sim$200 °C, which corresponds to the formation of HNO_3 from the decomposition of cerium ammonium nitrate. It is reported that cerium ammonium nitrate decomposes to NO_2 starting at 185 °C which, in turn, reacts with H_2O to form HNO_3 and NO [37,38]. The formed HNO_3 then triggers the combustion reaction with the fuel, as noted elsewhere [24,25]. The reaction mixture also contains nickel nitrate but its decomposition to form HNO_3 occurs at higher temperature 252 °C [39], hence it is not the trigger for ignition in the present case. In contrast, the ignition temperature of hydrous hydrazine fuel is $\sim$120 °C and is related to its boiling point ($\sim$114 °C), with subsequent reaction of the fuel vapor with ambient oxygen [25].

The influence of Ni loading and ϕ value on the combustion characteristics is also presented in Table 1, with hydrous hydrazine used as fuel. With increase of Ni loading from 3 to 68 wt%, the maximum measured temperature and amount of gases evolved during combustion decrease. On the other hand, with increasing ϕ, the intensity of combustion becomes significantly stronger and the amount of gases increases. These trends for the effects of Ni loading and ϕ follow the predictions for the adiabatic case.
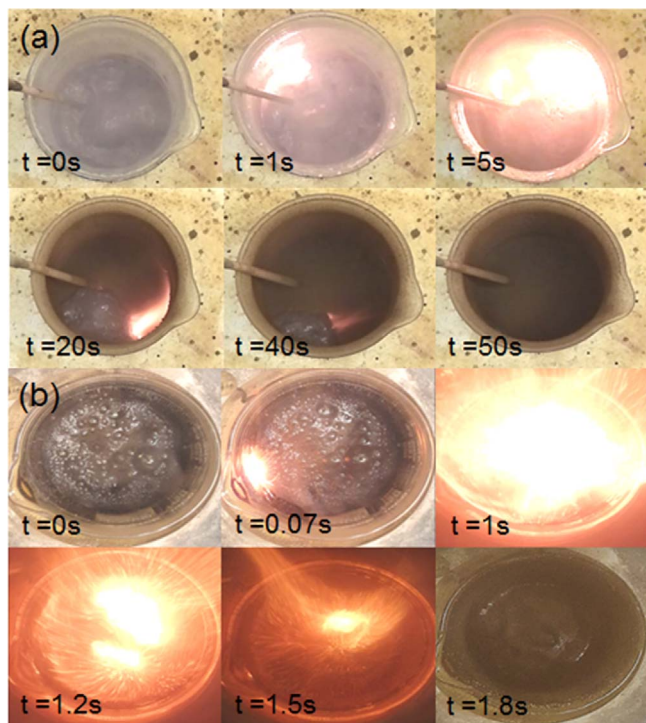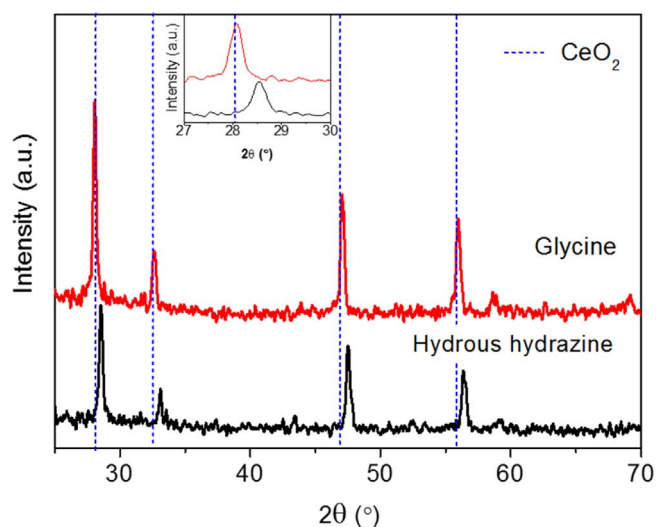
3.2. Catalyst characterization

The XRD patterns of the 6 wt% Ni/CeO_2 catalysts prepared with different fuels at $\phi = 2$ are shown in Fig. 3. Both catalysts clearly exhibit the CeO_2 phase (JCPDS No. 43-1002) while Ni phase was not observed, which suggests that Ni particles are highly dispersed on the support. However, the possibility also exists that the Ni content is too low to be detected by the XRD analysis. It is evident that peaks corresponding to CeO_2 phase for the glycine fuel are sharper than those for the hydrous hydrazine fuel, indicating the higher crystallinity of CeO_2 phase. Considering that the maximum temperature with glycine fuel (1150 °C) is higher than with hydrous hydrazine fuel (940 °C), the difference of crystallinity for the two catalysts is in agreement with the combustion characteristics. In addition, it is noticeable that the peaks of CeO_2 phase in 6 wt% Ni/CeO_2-HH-2 significantly shift to higher degrees relative to those for the reference, whereas the peak shifting is less obvious in 6 wt% Ni/CeO_2-GL-2 catalyst. This peak shifting which indicates the lattice contraction can be due to the partial incorporation of smaller Ni^{2+} ions ($r_{Ni} = 0.81$ Å) into the lattice of Ce^{4+} ($r_{Ce} = 0.97$ Å) to form a Ni−O−Ce solid solution [40]. Liu et al. reported that the formation of such solid solution is favorable at lower calcination temperature and it may decompose with high-temperature calcination [41]. Thus, the higher maximum temperature with glycine fuel may hinder the formation of Ni−O−Ce solid solution. It is known that formation of the solid solution yields the oxygen vacancies due to the charge unbalance and lattice distortion caused by the differences between the radii and oxidation states of Ni^{2+} and Ce^{4+} ions [42–44].

Table 1
Combustion characteristics of catalysts as a function of Ni loading, fuel-to-oxidizer ratio and fuel.

Sample	Maximum temperature (°C)		Amount of produced gases (mol)
	Measured	Adiabatic	
3 wt% Ni/CeO$_2$-HH-2	1100	1650	27.5
6 wt% Ni/CeO$_2$-HH-2	940	1587	26.2
13 wt% Ni/CeO$_2$-HH-2	795	1470	23.7
24 wt% Ni/CeO$_2$-HH-2	800	1310	20.6
68 wt% Ni/CeO$_2$-HH-2	754	933	13.9
6 wt% Ni/CeO$_2$-HH-0.5	396	687	21.7
6 wt% Ni/CeO$_2$-HH-1	454	1046	23.2
6 wt% Ni/CeO$_2$-HH-3	1225	1931	29.2
6 wt% Ni/CeO$_2$-GL-2	1150	1770	24.0

Fig. 2. Combustion process for different fuel systems (a) hydrous hydrazine, and (b) glycine.

Fig. 3. XRD patterns of 6 wt% Ni/CeO$_2$-HH-2 and 6 wt% Ni/CeO$_2$-GL-2 catalysts, compared with the reference of CeO$_2$ (JCPDS No. 43-1002).

This oxygen vacancy in the Ni−O−Ce solid solution of Ni/CeO$_2$ catalysts modifies the electronic ability of Ni as an electron donor and alters the interaction between the Ni and N$_2$H$_4$ molecules, which facilitates N−H bond dissociation instead of N−N bond on Ni and makes the H$_2$ generation easier [17].

For the XRD patterns of the 6 wt% Ni/CeO$_2$-HH-*z* catalysts prepared at different ϕ values (Fig. S4), the peaks of CeO$_2$ phase become sharper and stronger as ϕ increases, indicating that the crystallinity of CeO$_2$ phase increases. In addition, the peak shifting is more pronounced for the catalysts prepared at low ϕ value. The change of crystallinity and peak shifting with variation of ϕ is reasonable considering that the maximum temperature increases with an increase of ϕ value. The XRD patterns of the Ni/CeO$_2$-HH-2 catalysts with different Ni loading (Fig. S5) clearly show the Ni phase (JCPDS No. 04-0850) as well as the CeO$_2$ phase. As expected, the intensity of peaks for Ni phase diminishes with a decrease of Ni loading and the Ni phase was not found for 3 and 6 wt % Ni/CeO$_2$-HH-2 catalysts, possibly due to the high dispersion of Ni particles or the resolution limit of XRD measurement. It may be seen that the peak shifting of CeO$_2$ peaks towards higher degrees is more pronounced for the catalysts with lower Ni loading. Thus, although higher measured maximum temperature was observed at lower Ni loading, it appears that the formation of Ni−O−Ce solid solution is favored at lower Ni loading. It has been reported that, owing to segregation of Ni particles, formation of the solid solution is less favorable with increase in Ni loading [45,46]. This implies that the formation of Ni−O−Ce solid solution depends on combustion temperature as well as Ni loading, and is more strongly affected by the Ni loading than the combustion temperature.

The morphologies of the catalysts were observed by TEM analysis (Fig. 4). The mean Ni particle size and size distribution histograms of the catalysts, obtained from TEM images, are presented in Table 2 and Fig. S6, respectively. The images show Ni particle size ranging from 10.3 to 38.9 nm, close to those calculated from the XRD patterns using the Scherrer equation [47]. It may be seen that the catalyst using hydrous hydrazine fuel has smaller Ni particle size than that prepared using glycine fuel, due to the lower maximum temperature which decreases agglomeration and sintering of particles [23]. Similarly, the Ni particle size of the catalysts increases with increase of ϕ value. With an increase of Ni loading from 3 to 6 wt%, the Ni particle size decreases due to the smaller maximum temperature. When the Ni loading increases further, however, the Ni particle size increases significantly despite a decrease of the maximum temperature. It appears that for higher Ni loadings (13–68 wt%), the effect of nickel segregation dominates the heating effect by combustion.

The BET surface areas and pore sizes for all catalysts are also presented in Table 2. The BET surface areas are in the range 5.2–14.7 m^2/g, although there was no clear trend with the combustion characteristics. The pore size, on the other hand, increases with increased amount of gases released during combustion. For samples with high maximum temperature above 1100 °C, however, shrinkage of pore structure occurred regardless of the level of gas evolution owing to
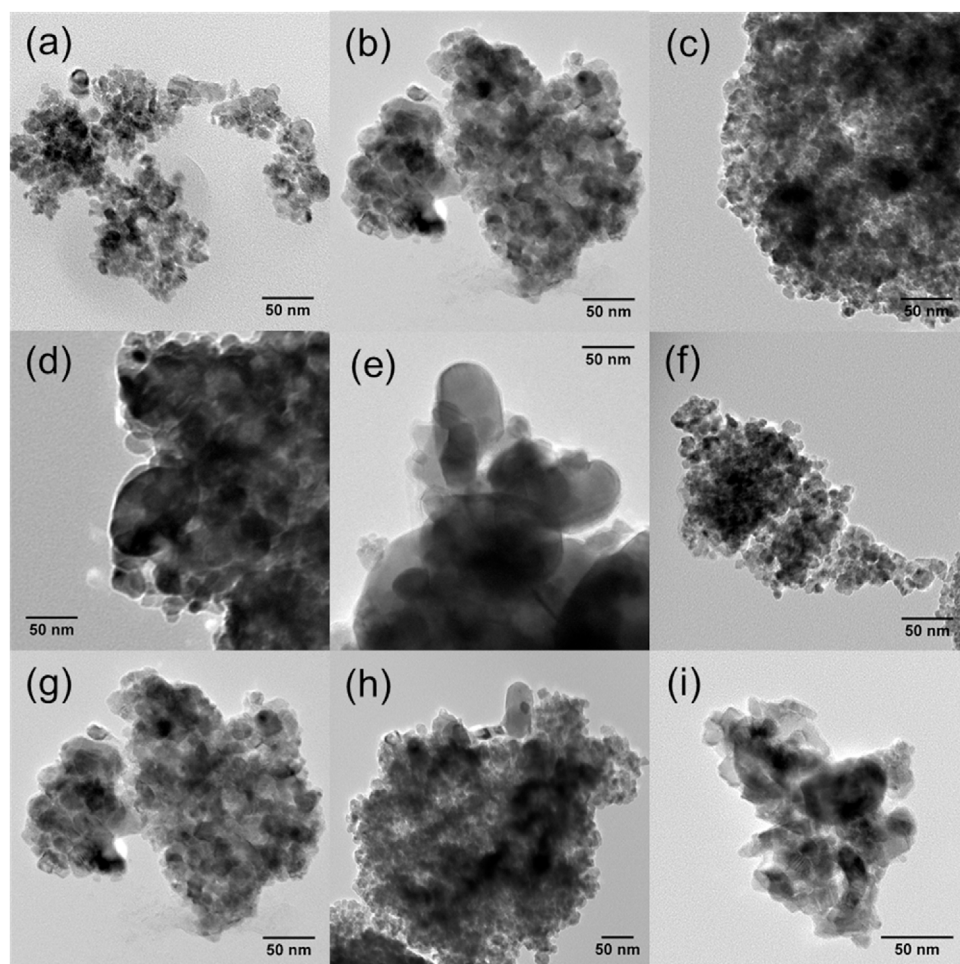
Fig. 4. TEM images of different catalysts. (a) 3 wt% Ni-CeO$_2$-HH-2, (b) 6 wt% Ni-CeO$_2$-HH-2 (c) 13 wt% Ni-CeO$_2$-HH-2, (d) 24 wt% Ni-CeO$_2$-HH-2, (e) 68 wt % Ni-CeO$_2$-HH-2, (f) 6 wt% Ni-CeO$_2$-HH-0.5, (g) 6 wt% Ni-CeO$_2$-HH-1, (h) 6 wt% Ni-CeO$_2$-HH-3 and (i) 6 wt% Ni-CeO$_2$-GL-2.

Table 2
Physical properties of Ni/CeO$_2$ catalysts.

Sample	D_{Ni} (nm)		S_{BET} (m^2/g)	D_p (nm)
	XRD	TEM		
3 wt% Ni/CeO$_2$-HH-2	NA	16.5	10.2	16.6
6 wt% Ni/CeO$_2$-HH-2	NA	14.7	12.5	18.8
13 wt% Ni/CeO$_2$-HH-2	20.9	19.2	14.7	15.5
24 wt% Ni/CeO$_2$-HH-2	23.1	23.9	13.8	15.2
68 wt% Ni/CeO$_2$-HH-2	37.4	38.9	6.8	12.7
6 wt% Ni/CeO$_2$-HH-0.5	NA	10.3	12.0	14.8
6 wt% Ni/CeO$_2$-HH-1	NA	11.9	12.1	15.7
6 wt% Ni/CeO$_2$-HH-3	NA	17.5	5.2	17.0
6 wt% Ni/CeO$_2$-GL-2	NA	16.2	11.9	13.2

sintering. In such cases, the heating effect by combustion dominates the heat dissipation by gas evolution. Consequently, among the investigated catalysts in this study, 6 wt% Ni/CeO$_2$-HH-2 catalyst has the largest pore size (18.8 nm).

The reducibility of the samples was investigated using H$_2$-TPR experiments to confirm the interaction between Ni and CeO$_2$, namely existence of the Ni−O−Ce solid solution. The H$_2$-TPR profiles of 6 wt% Ni/CeO$_2$-HH-2 and 6 wt% Ni/CeO$_2$-GL-2 samples are shown in Fig. 5. For the sample prepared with hydrous hydrazine fuel, two hydrogen consumption peaks (α and β) were observed while, in contrast, only the β peak was observed for the sample prepared with glycine fuel. The α peak is due to the reduction of adsorbed oxygen which is linked to the oxygen vacancy on the Ni−O−Ce solid solution, while the β peak corresponds to the reduction of NiO particles [44]. This feature indicates
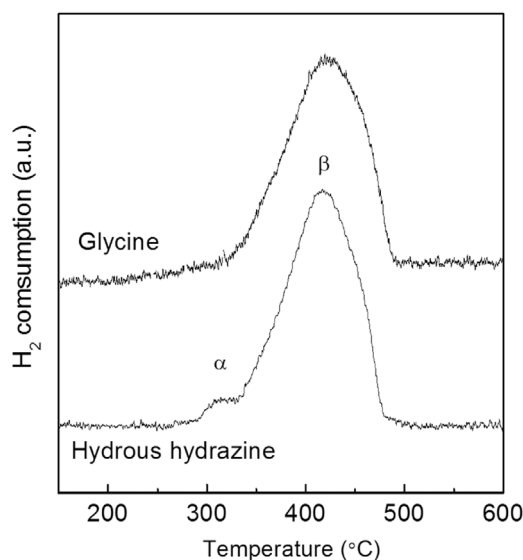

Fig. 5. H$_2$-TPR profiles of 6 wt% Ni/CeO$_2$-HH-2 and 6 wt% Ni/CeO$_2$-GL-2 samples.

that hydrous hydrazine fuel produces larger amount of Ni−O−Ce solid solution while it is low or negligible for glycine fuel. This result agrees with the XRD analysis. Moreover, the β peak of 6 wt% Ni/CeO$_2$-GL-2 is positioned at slightly higher temperature as compared to that of 6 wt% Ni/CeO$_2$-HH-2. This indicates presence of larger NiO particles which are more difficult to reduce, and agrees with the average Ni particle sizes obtained from TEM analysis. As noted above, smaller Ni particle

size and larger amount of solid solution for 6 wt% Ni/CeO$_2$-HH-2 are both attributed to the relatively milder combustion characteristics.

The H$_2$-TPR profiles of 6 wt% Ni/CeO$_2$ samples prepared at different ϕ (Fig. S7) shows that the intensity of α peak decreases while the β peak shifts to higher temperatures with increasing ϕ values. These features further confirm that the formation of Ni−O−Ce solid solution becomes more unfavorable, while the Ni particle size increases, with increase of maximum temperature during SCS. The H$_2$-TPR profiles of samples with different Ni loadings (Fig. S8) illustrate that the concentration of Ni−O−Ce solid solution depends on the Ni loading. For the samples with 68 and 24 wt% Ni loading, no α peak was observed. As the Ni content decreases to 13 wt%, the α peak appears and its area increases slightly with a decrease from 13 to 6 wt%. This indicates that the formation of Ni−O−Ce solid solution is favorable at lower Ni loading, which agrees with the XRD results. For the sample with 3 wt% Ni loading, the area of the α peak is slightly smaller than for 6 wt% Ni loading and the γ peak is found, which is responsible for the reduction of oxygen vacancies of free CeO$_2$ [42]. This implies that 3 wt% Ni loading leads to lower Ni−O−Ce solid solution and is not sufficiently high for Ni particles to cover the CeO$_2$ phase. The temperature for the β peak generally increases with Ni loading, with the exception of 6 wt% sample, suggesting that it has the smallest Ni particle size which is confirmed from the TEM and XRD analysis shown in Table 2. Prior studies also reported a minimum Ni loading for the highest metal dispersion in Ni/CeO$_2$ catalysts [42,48].

3.3. Catalytic performance for hydrous hydrazine decomposition

The catalytic performance of different Ni/CeO$_2$ catalysts for hydrous hydrazine decomposition was evaluated at 50 °C [n(Ni)/n(N$_2$H$_4$) = 0.1] and is summarized in Table 3. It was found that the catalytic activity and selectivity for hydrogen generation depend strongly on the SCS synthesis parameters (ratio of precursor oxidizers, ϕ value and fuel type). This finding aligns with the trend of physicochemical properties such as Ni particle size, pore size and amount of Ni−O−Ce solid solution by changing the SCS synthesis parameters. In summary, catalysts with smaller Ni particle size, larger pore size and higher concentration of Ni−O−Ce solid solution show good catalytic performance. Too much concentration of the solid solution, however, was unfavorable for the catalytic performance because the solid solution acts as a promoter but not an active site by itself [17]. It is well known that small metal particle size increases the number of active sites [49], larger pore size improves mass transport within pores [50], and Ni−O−Ce solid solution can enhance catalytic activity and H$_2$ selectivity of Ni/CeO$_2$ catalysts by modifying the electronic properties of nearby metallic Ni [17,51,52]. The best catalytic activity was observed for the 6 wt% Ni/CeO$_2$-HH-2 catalyst, for which the reaction took 17.7 min for 50% conversion of hydrous hydrazine, corresponding to a TOF value of 34.0 h^{-1}. Also, its H$_2$ selectivity was 100%, with the product gas containing only H$_2$ and N$_2$ in the molar ratio H$_2$/N$_2$ = 2. This catalytic

Table 3
Catalytic performance of Ni/CeO$_2$ catalysts for hydrous hydrazine decomposition [n(Ni)/n(N$_2$H$_4$) = 0.1, 50 °C].

Sample	H$_2$ selectivity (%)	TOF (h^{-1})[a]
3 wt% Ni/CeO$_2$-HH-2	100	20.9 ± 0.7
6 wt% Ni/CeO$_2$-HH-2	100	34.0 ± 1.9
13 wt% Ni/CeO$_2$-HH-2	99	21.8 ± 1.2
24 wt% Ni/CeO$_2$-HH-2	99	22.3 ± 1.9
68 wt% Ni/CeO$_2$-HH-2	95	5.1 ± 0.1
6 wt% Ni/CeO$_2$-HH-0.5	94	21.1 ± 0.9
6 wt% Ni/CeO$_2$-HH-1	100	29.0 ± 0.6
6 wt% Ni/CeO$_2$-HH-3	98	26.6 ± 1.3
6 wt% Ni/CeO$_2$-GL-2	98	19.6 ± 1.4

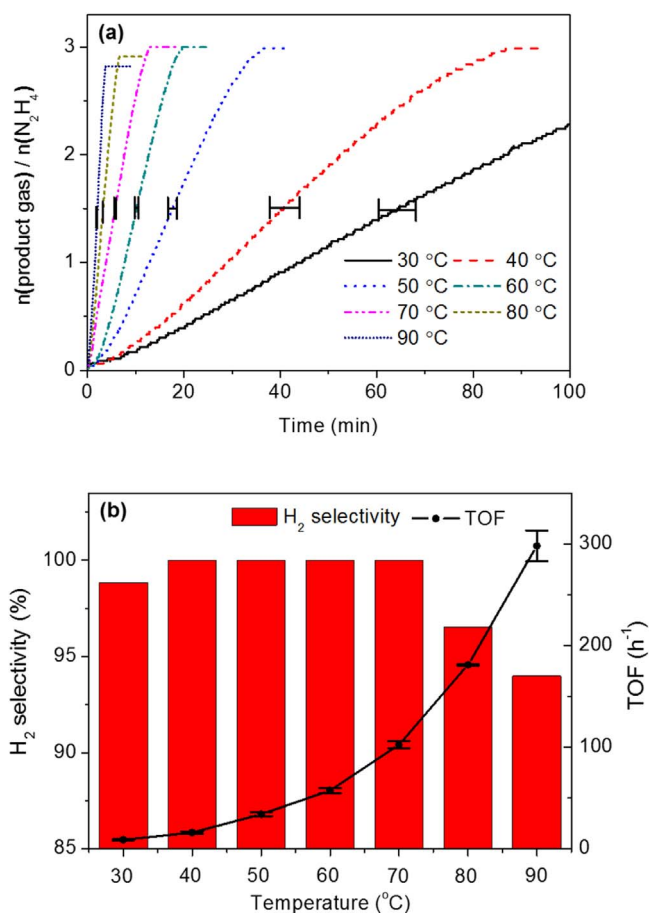[a] TOFs were calculated at 50% conversion of hydrous hydrazine.

Fig. 6. (a) Time-course profiles and (b) H$_2$ selectivity and TOF values for the decomposition of hydrous hydrazine over 6 wt% Ni/CeO$_2$-HH-2 catalyst as a function of temperature [n(Ni)/n(N$_2$H$_4$) = 0.1].
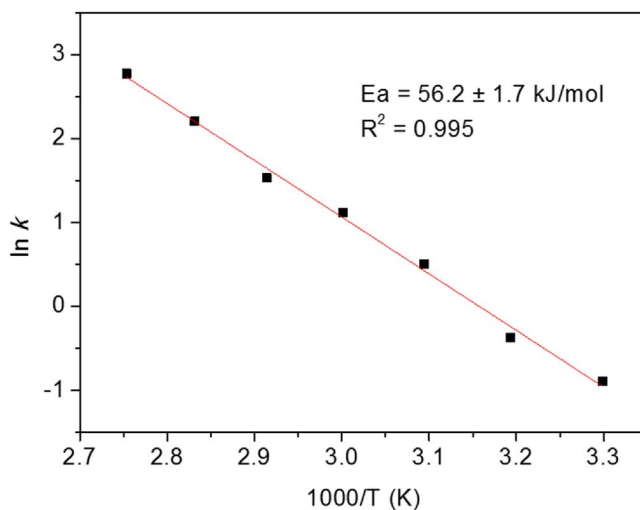

Fig. 7. Arrhenius plot showing the apparent activation energy for hydrous hydrazine decomposition over 6 wt% Ni/CeO$_2$-HH-2 catalyst.

performance may be related to its physicochemical properties such as relatively small Ni particle size (14.7 nm), large pore size (18.8 nm) and moderate concentration of Ni−O−Ce solid solution.

The hydrous hydrazine decomposition plots over the 6 wt% Ni/CeO$_2$-HH-2 catalyst at different temperatures are shown in Fig. 6. As expected, the reaction rate significantly increased about 30-fold with increase of reaction temperature from 30 to 90 °C (Fig. 6a). The

W. Kang, A. Varma

Table 4
Comparison of catalytic performance of different Ni-based catalysts for hydrous hydrazine decomposition.

Catalyst	Preparation method	Reaction conditions		H_2 selectivity (%)	TOF (h^{-1})	Ref.
		Metal/N_2H_4 molar ratio	T (°C)			
6 wt% Ni/CeO$_2$[a]	SCS	0.1	30	99	9.2	This study
		0.1	50	100	34.0	
Ni (53.4 wt%)-0.08CeO$_2$	Co-precipitation	0.45	30	99	4.0	[13]
		0.45	50	99	20.3	
Ni (18.3 wt%)/CeO$_2$	Impregnation	0.45	30	65	1.2	[13]
Ni (67.7 mol%)/meso-CeO$_2$	one-pot EISA	0.1	30	97	5.1	[14]
Ni (78 wt%)-Al$_2$O$_3$-HT	Co-precipitation	0.42	50	93	26.3	[49]

[a] Refers to the 6 wt% Ni/CeO$_2$-HH-2 catalyst.

reaction times for 50% conversion were 67.0 ± 3.9, 5.9 ± 0.2, and 1.9 ± 0.1 min at 30, 70 and 90 °C, respectively. The standard deviation of the reaction time for 50% conversion is indicated by the error bars in Fig. 6a. As shown in Fig. 6b, the selectivity to hydrogen generation is 99% at 30 °C and remains 100% in the temperature range 40–70 °C. When the temperature increases further to 90 °C, the H_2 selectivity decreases sharply to 93% owing to thermodynamic reasons, as reported elsewhere [53,54]. The TOFs for 50% conversion are shown in Fig. 6b and reported in Table S2. Based on these data, the apparent activation energy (Ea) for catalytic decomposition of hydrous hydrazine over the 6 wt% Ni/CeO$_2$-HH-2 catalyst was determined to be 56.2 ± 1.7 kJ/mol (Fig. 7), which compares well with values for Ni-based catalysts reported in the literature [18,51,52,55]. In recycling tests to assess catalyst reusability, the 6 wt% Ni/CeO$_2$-HH-2 catalyst retained 100% H_2 selectivity over 3 cycles and exhibited relatively small decrease in catalytic activity, which has also been observed by others (Fig. S10) [11,36,53].

The performance of the 6 wt% Ni/CeO$_2$-HH-2 catalyst was compared to other Ni catalysts synthesized by different methods (Table 4). Although a rigorous comparison is difficult due to the variety of experimental conditions utilized, it indicates that the catalyst prepared by SCS has higher activity, along with high H_2 selectivity. The high activity of the catalyst prepared by SCS arises in part from the highly porous structure which is a typical feature of SCS products. As compared to the Ni/CeO$_2$ catalyst prepared by one-pot EISA method [18], the pore size of the 6 wt% Ni/CeO$_2$-HH-2 catalyst is 6 times larger, which facilitates the accessibility of reactants to the catalyst active sites. It is a possible reason why the 6 wt% Ni/CeO$_2$-HH-2 catalyst of this study exhibits better performance even though the Ni content is much lower than in other works, providing an economic advantage. To our knowledge, the catalyst developed in this study provides the highest performance among all catalysts containing Ni alone. It is known, however, that addition of noble metals significantly enhances the performance of Ni-based catalysts [18,20,21,34]. A current challenge is to develop other non-noble metal containing catalysts that exhibit good performance [56] and this work is currently underway.

4. Conclusions

In this work, for the first time, SCS was used to prepare Ni/CeO$_2$ catalysts for efficient hydrogen generation from hydrous hydrazine, a promising hydrogen carrier for fuel cell vehicles. By varying the SCS synthesis parameters in terms of ratio of precursor oxidizers (nickel nitrate and ammonium cerium nitrate), fuel-to-oxidizer ratio (ϕ) and fuel type (hydrous hydrazine and glycine), the correlation between combustion characteristics, physicochemical and catalytic properties was investigated in detail. The catalyst characterization demonstrates that Ni particle size, pore structure and amount of Ni−O−Ce solid solution depend strongly on the combustion features, including maximum temperature and amount of gas evolution. The use of hydrous hydrazine fuel with $\phi = 2$ allows to obtain 6 wt% Ni powders with small Ni

particle size (14.7 nm), large pore size (18.8 nm) and moderate concentration of Ni−O−Ce solid solution which promote the catalytic performance for hydrogen generation. This material exhibited 100% H_2 selectivity and TOF value of 34.0 h^{-1} at 50 °C, which is the highest activity among all catalysts tested in this study and all catalysts containing Ni alone reported in the literature. This work demonstrates that SCS is an effective method to prepare catalysts for selective hydrogen generation from hydrous hydrazine decomposition at moderate temperatures for fuel cell vehicle applications. It is also an example which demonstrates that understanding the influence of SCS parameters on combustion characteristics and their correlation with product properties can enable one to effectively control the combustion process and to tailor catalysts for specific applications.

Appendix A. Supplementary data

Supplementary data associated with this article can be found, in the online version, at http://dx.doi.org/10.1016/j.apcatb.2017.08.053.

References

[1] H.T. Hwang, A. Varma, Curr. Opin. Chem. Eng. 5 (2014) 42–48.
[2] M. Yadav, Q. Xu, Energy Environ. Sci. 5 (2012) 9698–9725.
[3] E.W. Schmidt, Hydrazine and Its Derivatives: Preparation, Properties, Applications, 2nd ed., Wiley, New York, 2001.
[4] Q.L. Zhu, Q. Xu, Energy Environ. Sci. 8 (2015) 478–512.
[5] R. Halseid, P.J.S. Vie, R. Tunold, J. Power Sources 154 (2006) 343–350.
[6] X. Cheng, Z. Shi, N. Glass, L. Zhang, J.J. Zhang, D.T. Song, Z.S. Liu, H.J. Wang, J. Shen, J. Power Sources 165 (2007) 739–756.
[7] S.K. Singh, X.B. Zhang, Q. Xu, J. Am. Chem. Soc. 131 (2009) 9894–9895.
[8] S.K. Singh, Q. Xu, J. Am. Chem. Soc. 131 (2009) 18032–18033.
[9] S.K. Singh, Y. Iizuka, Q. Xu, Int. J. Hydrogen Energy 36 (2011) 11794–11801.
[10] K.V. Manukyan, A. Cross, S. Rouvimov, J. Miller, A.S. Mukasyan, E.E. Wolf, Appl. Catal. A-Gen. 476 (2014) 47–53.
[11] D. Bhattacharjee, S. Dasgupta, J. Mater. Chem. A 3 (2015) 24371–24378.
[12] H.-L. Wang, J.-M. Yan, Z.-L. Wang, S.-I. O, Q. Jiang, J. Mater. Chem. A 1 (2013) 14957–14962.
[13] O. Song-Il, J.-M. Yan, H.-L. Wang, Z.-L. Wang, Q. Jiang, Int. J. Hydrogen Energy 39 (2014) 3755–3761.
[14] J.-K. Sun, Q. Xu, ChemCatChem 7 (2015) 526–531.
[15] L. He, Y.Q. Huang, A.Q. Wang, Y. Liu, X.Y. Liu, X.W. Chen, J.J. Delgado, X.D. Wang, T. Zhang, J. Catal. 298 (2013) 1–9.
[16] N. Firdous, N.K. Janjua, I. Qazi, M.H. Sarwar Wattoo, Int. J. Hydrogen Energy 41 (2016) 984–995.
[17] L. He, B.L. Liang, L. Li, X.F. Yang, Y.Q. Huang, A.Q. Wang, X.D. Wang, T. Zhang, ACS Catal. 5 (2015) 1623–1628.
[18] Y.-Y. Jiang, H.-B. Dai, Y.-J. Zhong, D.-M. Chen, P. Wang, Chem. Eur. J. 21 (2015) 15439–15445.
[19] S.I. O, J.M. Yan, H.L. Wang, Z.L. Wang, Q. Jiang, J. Power Sources 262 (2014) 386–390.

[20] Y.J. Zhong, H.B. Dai, M. Zhu, P. Wang, Int. J. Hydrogen Energy 41 (2016) 11042–11049.
[21] B.Q. Xia, T. Liu, W. Luo, G.Z. Cheng, J. Mater. Chem. A 4 (2016) 5616–5622.
[22] L. He, Y. Huang, X.Y. Liu, L. Li, A. Wang, X. Wang, C.-Y. Mou, T. Zhang, Appl. Catal. B: Environ. 147 (2014) 779–788.
[23] A. Varma, A.S. Mukasyan, A.S. Rogachev, K.V. Manukyan, Chem. Rev. 116 (2016) 14493–14586.
[24] P. Erri, P. Pranda, A. Varma, Ind. Eng. Chem. Res. 43 (2004) 3092–3096.
[25] K. Deshpande, A. Mukasyan, A. Varma, Chem. Mater. 16 (2004) 4896–4904.
[26] T. Striker, J.A. Ruud, J. Am. Ceram. Soc. 93 (2010) 2622–2629.
[27] K.V. Manukyan, A. Cross, S. Roslyakov, S. Rouvimov, A.S. Rogachev, E.E. Wolf, A.S. Mukasyan, J. Phys. Chem. C 117 (2013) 24417–24427.
[28] R. Ghose, H.T. Hwang, A. Varma, Appl. Catal. A-Gen. 472 (2014) 39–46.
[29] A. Vita, C. Italiano, C. Fabiano, M. Lagana, L. Pino, Mater. Chem. Phys. 163 (2015) 337–347.
[30] Y. Gao, F.H. Meng, X. Li, J.Z. Wen, Z. Li, Catal. Sci. Technol. 6 (2016) 7800–7811.
[31] C. Aliotta, L.F. Liotta, V. La Parola, A. Martorana, E.N.S. Muccillo, R. Muccillo, F. Deganello, Appl. Catal. B: Environ. 197 (2016) 14–22.
[32] A.A. Shiryaev, Int. J. SHS 4 (1995) 351–362.
[33] S.K. Singh, Z.H. Lu, Q. Xu, Eur. J. Inorg. Chem. (2011) 2232–2237.
[34] F.Z. Song, Q.L. Zhu, Q. Xu, J. Mater. Chem. A 3 (2015) 23090–23094.
[35] Q.L. Zhu, D.C. Zhong, U.B. Demirci, Q. Xu, ACS Catal. 4 (2014) 4261–4268.
[36] J.M. Chen, Q.L. Yao, J. Zhu, X.S. Chen, Z.H. Lu, Int. J. Hydrogen Energy 41 (2016) 3946–3954.
[37] G. Pokol, T. Leskela, L. Niinisto, J. Therm. Anal. 42 (1994) 343–359.
[38] F. Vratny, S. Kern, F. Gugliotta, J. Inorg. Nucl. Chem. 17 (1961) 281–285.
[39] A. Kumar, E.E. Wolf, A.S. Mukasyan, AIChE J. 57 (2011) 2207–2214.
[40] R. Shannon, Acta Crystallogr. A 32 (1976) 751–767.
[41] X. Liu, Y. Zuo, L. Li, X. Huang, G. Li, RSC Adv. 4 (2014) 6397–6406.
[42] P.V.R. Rao, V.P. Kumar, G.S. Rao, K.V.R. Chary, Catal. Sci. Technol. 2 (2012) 1665–1673.
[43] S. Pengpanich, V. Meeyoo, T. Rirksomboon, Catal. Today 93–95 (2004) 95–105.
[44] W.J. Shan, M.F. Luo, P.L. Ying, W.J. Shen, C. Li, Appl. Catal. A-Gen. 246 (2003) 1–9.
[45] L. Jalowiecki-Duhamel, H. Zarrou, A. D'Huysser, Int. J. Hydrogen Energy 33 (2008) 5527–5534.
[46] C. Lamonier, A. Ponchel, A. D'Huysser, L. Jalowiecki-Duhamel, Catal. Today 50 (1999) 247–259.
[47] B.D. Cullity, S.R. Stock, Elements of x-ray Diffraction, 3rd ed., Prentice Hall, Upper Saddle River, NJ, 2001 (xviii, 678 p.).
[48] P. Biswas, D. Kunzru, Int. J. Hydrogen Energy 32 (2007) 969–980.
[49] G. Ertl, H. Knèozinger, J. Weitkamp, Handbook of Heterogeneous Catalysis, VCH, Weinheim, 1997.
[50] M.E. Davis, R.J. Davis, Fundamentals of Chemical Reaction Engineering, 1st ed., McGraw-Hill, Boston, 2003 (p xvi, 368 p.).
[51] Y.Y. Jiang, Q. Kang, J.J. Zhang, H.B. Dai, P. Wang, J. Power Sources 273 (2015) 554–560.
[52] Z.J. Zhang, Z.H. Lu, H.L. Tan, X.S. Chen, Q.L. Yao, J. Mater. Chem. A 3 (2015) 23520–23529.
[53] L. He, Y.Q. Huang, A.Q. Wang, X.D. Wang, X.W. Chen, J.J. Delgado, T. Zhang, Angew. Chem. Int. Ed. 51 (2012) 6191–6194.
[54] L. He, Y.Q. Huang, A.Q. Wang, X.D. Wang, T. Zhang, AIChE J. 59 (2013) 4297–4302.
[55] Y.-J. Zhong, H.-B. Dai, Y.-Y. Jiang, D.-M. Chen, M. Zhu, L.-X. Sun, P. Wang, J. Power Sources 300 (2015) 294–300.
[56] S.K. Singh, A.K. Singh, K. Aranishi, Q. Xu, J. Am. Chem. Soc. 133 (2011) 19638–19641.